Chitosan/Nanohydroxyapatite/Hydroxyethyl-cellulose-based printable formulations for local alendronate drug delivery in osteoporosis treatment

Afra, Simindokht; Koch, Marcus; Żur-Pińska, Joanna; Dolatshahi, Maryam; Bahrami, Ahmad Reza; Sayed, Julien Es; Moradi, Ali; Matin, Maryam M.; Włodarczyk-Biegun, Małgorzata Katarzyna

Published in:
Carbohydrate Polymer Technologies and Applications

DOI:
10.1016/j.carpta.2023.100418

Publication date:
2024

Carbohydrate Polymer Technologies and Applications 7 (2024) 100418

Contents lists available at ScienceDirect

Carbohydrate Polymer Technologies and Applications

journal homepage: www.sciencedirect.com/journal/carbohydrate-polymer-technologies-and-applications

Chitosan/Nanohydroxyapatite/Hydroxyethyl-cellulose-based printable formulations for local alendronate drug delivery in osteoporosis treatment

Simindokht Afra [a,b], Marcus Koch [c], Joanna Żur-Pińska [b], Maryam Dolatshahi [a], Ahmad Reza Bahrami [a,d], Julien Es Sayed [e], Ali Moradi [f], Maryam M. Matin [a,g,*], Małgorzata Katarzyna Włodarczyk-Biegun [b,e,*]

[a] Department of Biology, Faculty of Science, Ferdowsi University of Mashhad, Azadi Square, 9177948974, Mashhad, Iran
[b] Biotechnology Centre, Silesian University of Technology, B. Krzywoustego 8, 44-100 Gliwice, Poland
[c] INM – Leibniz Institute for New Materials, Campus D2 2, 66123 Saarbrücken, Germany
[d] Industrial Biotechnology Research Group, Institute of Biotechnology, Ferdowsi University of Mashhad, Mashhad, Iran
[e] Polymer Science, Zernike Institute for Advanced Materials, University of Groningen, Nijenborgh 4, 9747 AG Groningen, the Netherlands
[f] Orthopedic Research Center, Department of Orthopedic Surgery, Mashhad University of Medical Sciences, 91388-13944, Mashhad, Iran
[g] Novel Diagnostics and Therapeutics Research Group, Institute of Biotechnology, Ferdowsi University of Mashhad, Azadi Square, 9177948974, Mashhad, Iran

ARTICLE INFO

Keywords:
Chitosan
3D bioprinting
Osteoporosis
Alendronate
Osteoclastogenesis

ABSTRACT

Osteoporosis is a silent bone disease and a growing health issue. Despite recent progress in diagnosis and treatment, effective therapeutic strategies are still needed. One of the possible solutions is the implantation of engineered drug-releasing scaffolds at the disease site. To boost this approach further, we aimed to develop printable materials (the inks) for the construction of patient-specific 3D scaffolds with drug-release capability. The inks were composed of chitosan – a natural osteoinductive polysaccharide, nanohydroxyapatite – a natural bone matrix ingredient improving mechanical properties, sodium alendronate – a bioactive drug, and hydroxyethyl-cellulose – a filler improving the printability. Printed scaffolds were crosslinked with citric acid or KOH. After coating with collagen and gelatin, they demonstrated biocompatibility with the adipose-derived mesenchymal stem cells and MG-63 cell line. They also showed a sustained release of alendronate for 50 days, causing a significant reduction in the expression of *Cathepsin K*, an osteoclast-specific gene marker, which indicates the osteoclast-inhibiting capacity of the coated scaffolds. This work demonstrates the potential of developed printable materials to find applications as cell and drug carriers for the treatment of osteoporosis.

1. Introduction

Osteoporosis (OS) is a disease recognized by a great loss in mineral bone mass (Paspaliaris & Kolios, 2019) with an incidence of one in 3 seconds (Reid, 2020). Moreover, this number is expected to double by 2040 (Adami et al., 2022; de Villiers & Goldstein, 2022; Shen et al., 2022). Although bones have high natural tissue regeneration capacity, in some cases, such as large and severe bone defects, tumors, and metabolic bone diseases, full recovery of the initial bone strength and structure is not possible. In osteoporosis, the dysregulation of regeneration capacity is caused by the imbalance between bone resorption and new bone formation, which effectively leads to loss of bone mass. The most common fracture sites caused by osteoporosis are distal forearm, proximal humerus, hip, and spine fractures (Bone et al., 2017; Jing et al., 2016).

Several factors are involved in the initiation and progression of osteoporosis including, hormonal, nutritional, and genetic factors (Fuggle et al., 2019), meanwhile the most important and indispensable reason is aging. All these playing factors are thought to change the balance between two main proteins of receptor activator of nuclear factor kappa-B ligand (RANKL) and osteoprotegerin (OPG). The latter can bind to RANKL and prevent the ligand binding to RANK, leading to bone resorption. The higher amount of RANKL can be caused by a dwindling of steroid hormones (estrogen and progesterone in women and testosterone in men) resulting in pre-osteoclast maturation. The balance of OPG and RANKL proteins maintains the proper regeneration capacity of bones (McClung, 2007; Mizuno et al., 1998; Owen & Reilly, 2018).

* Corresponding authors.
E-mail addresses: Matin@um.ac.ir (M.M. Matin), malgorzata.wlodarczyk-biegun@polsl.pl, m.k.wlodarczyk@rug.nl (M.K. Włodarczyk-Biegun).

https://doi.org/10.1016/j.carpta.2023.100418

Available online 2 January 2024

Osteoporosis treatment is divided into two main categories: pharmacological treatment and non-pharmacological management (Eastell et al., 2019). The first option of treatment, i.e. pharmacological therapy, including hormones, and drug therapy does not seem to be sufficient in progressive osteoporotic bones (Pavone et al., 2017). Bisphosphates are currently the main medication for osteoporosis. However, they are typically applied systemically, requiring longer time to reach to their target and have unwanted side effects. Despite their ability in inhibition of the disease (Jing et al., 2016; Kylloenen, D'Este, Alini, & Eglin, 2015), they cannot improve bone mass and bone strength at the sites with a high fracture incidence. Therefore, non-pharmacological management, including surgical approaches and bone grafting, was introduced. Autografts and allografts are common surgical approaches to induce bone renewal, especially in large defects (Wang & Yeung, 2017). However, these grafts have limitations in the quantity and quality of available sources, as well as often a need for another surgery and use of immuno-suppressants (Dimitriou, Mataliotakis, Angoules, Kanakaris, & Giannoudis, 2011). Therefore, patients with severe osteoporosis require new pre- and post-operative treatment plans (Kim, Park, Oh, & Choi, 2017), which could involve using engineered scaffolds containing drugs for sustainable *in situ* release.

3D (bio)printing allows production of scaffolds with well-controlled architecture and properties adjusted to the injury site. Hydrogels are widely explored materials for 3D (bio)printing (Mantha et al., 2019), due to their typical highly hydrated cell-friendly environment, and ability to transfer adequate gases, nutrients, and growth factors (Nallusamy & Das, 2021). In bone tissue engineering, the need for the development of hydrogels that can match the mechanical bone strength and mimic the natural bone environment is urging.

This study aimed to develop mechanically strong 3D printed hydrogel-based scaffolds for local drug delivery to offer better therapeutic solutions for osteoporosis treatment. To this aim, we prepared chitosan-based inks, containing chitosan (CS), nanohydroxyapatite (nHA), hydroxyethyl-cellulose (HEC), and the drug, alendronate (ALN). CS was chosen as a hydrophilic, non-toxic polymer with a structure that is similar to the glycosaminoglycans (GAGs) of extracellular matrix (ECM) (Bellich, D'Agostino, Semeraro, Gamini, & Cesàro, 2016; Islam, Shahruzzaman, Biswas, Nurus Sakib, & Rashid, 2020). HEC was added to improve the rheological properties of CS and enhance shape fidelity. To improve the mechanical aspect of the scaffolds, nHA was selected. It was also included as a major component of the inorganic mass of the ECM in native bones (Rajula, Narayanan, Venkatasubbu, Mani, & Sujana, 2021) to increase biocompatibility of the formulation (Ma et al., 2016). Finally, ALN, a bisphosphonate, was included as the active drug. The printability, biocompatibility, drug release and capability of scaffolds to inhibit osteoclastogenesis were tested. Using proposed drug-loaded scaffolds in the site of osteoporotic bones is envisioned to help in delaying the impact of the causative disease reasons.

2. Materials and methods

2.1. Materials

CS (medium molecular weight, 75–85 % deacetylation), nHA: < 200 nm, β-glycerol phosphate disodium salt hydrate (β-GP), acetic acid, potassium hydroxide (KOH), citric acid, HEC (average molecular weight ~720,000), ortho-phthaldialdehyde (OPA), 1-ethyl-3-(3-dimethylaminopropyl)carbodiimide (EDC), N-hydroxysuccinimide (NHS), 2-(N-morpholino)ethanesulfonic acid (MES) buffer, poly-D-lysine, collagen, phosphate-buffered saline (PBS) tablets, and penicillin/streptomycin were purchased from Sigma-Aldrich, USA. Methanol, 2-mercaptoethanol, and sodium hydroxide were analytical grade and purchased from Merck, Germany. Recombinant mouse soluble RANK ligand was purchased from ProSpec-Bio, USA. Dulbecco's modified Eagle's medium (DMEM), and glucose were provided by Gibco, USA and fetal bovine serum (FBS) by Thermo Fisher Scientific, USA.

2.2. Hydrogel preparation and 3D printing

Four different formulations were developed in this study, composed of: 1) CS, nHA, and β-GP (CS-BGP); 2) CS, nHA, HEC, and β-GP (CS-HEC-BGP); 3) CS, nHA, HEC, and KOH (CS-HEC-K).; 4) CS, nHA, HEC, and citric acid (CS-HEC-C). Detailed formulations are described in Table 1.

The highest dose (5 μg/ml) of ALN which is not toxic for the cells as estimated based on the MTT assay, was added to the formulations and used for drug-releasing scaffolds (for more details see Fig. 1 in SI).

The inks were prepared as follows: CS was dissolved in acetic acid solution (2 % v/v) at different percentages (3 %, 6 %, and 8 % w/v) at room temperature for 2 h under continuous stirring. ALN (5 μg/ml) and nHA (1.5 % w/v) were prepared in 2 % v/v acetic acid solution with sonication for 1 h. Afterwards, the nHA and ALN mixture was added dropwise to the CS solution and stirred magnetically overnight until a homogenous solution was achieved. Then, the pre-cooled (4 °C) β-GP solution (5x of final concentration) was added dropwise, up to the final concentration of 30 % (w/v) to neutralize the pH and introduce crosslinking. For the preparation of the CS-HEC-BGP, HEC was added in the last step at a concentration of 9 % (w/v). For the preparation of CS-HEC-K, 6 % w/v CS was dissolved in 2 % v/v acetic acid under magnetic stirring. nHA (1.5 % w/v)/ALN (5 μg/ml) mixture in 2 % v/v acetic acid was added dropwise to the CS solution. HEC powder was added in the last step at 6 % w/v, and mixed on a stirrer to form a homogenous hydrogel. KOH solution (1.5 M) was used as a crosslinker by soaking the scaffolds in the bath, post-printing for 1 min.

For the preparation of (CS-HEC-C), 9 % w/v CS and 20 % w/w of citric acid were mixed in 2 % v/v acetic acid under stirring. nHA (1.5 % w/v)/ALN (5 μg/ml) mixture in 2 % v/v acetic acid was added dropwise to that solution. HEC was added in the last step (9 % w/v) and mixed on a stirrer to reach a homogenous mixture. Fig. 1 shows a schematic representation of preparation of all 4 formulations.

Square-mesh (20 × 20 × 4 mm) and circle-formed scaffolds (20 mm diameter) were printed using an extrusion-based bio-printer with an infill percentage of 50 % (FELIX BIO-printer, the Netherlands). For the printing process, a conical nozzle with an inner diameter of 410 μm was used and the layer height was adjusted to 0.3 mm.

2.3. Crosslinking techniques

CS-BGP and CS-HEC-BGP were printed and then incubated at 37 °C with 5 % CO_2, for 15 min. The scaffold printed with CS-HEC-K, was post-printing cross-linked via soaking in 1.5 M KOH solution for 1 min at room temperature. This was followed by incubation in the oven at 165 °C for 20 min (see Fig. 1).

2.4. Rheological properties of inks

An HR-20 Rheometer (TA Instruments, New Castle, DE, USA) was used to characterize the inks. Strain sweep, frequency sweep, time sweep and recovery test were done for each ink before crosslinking. In addition, steady-shear viscosity measurement was performed to evaluate shear thinning properties of the inks. All tests were conducted at 25 °C

Table 1
Hydrogel formulations.

Abbreviation	Main ink composition (w/v)	Crosslinker/crosslinking procedure
1: CS-BGP	CS (3, 6 and 8 %) + nHA (1.5 %)	β-GP; incubation for 15 min at 37 °C
2:CS-HEC-BGP	CS (3 %) + nHA (1.5 %) + HEC (9 %)	β-GP; incubation for 15 min at 37 °C
3: CS-HEC-K	CS (6 %) + nHA (1.5 %) + HEC (6 %)	KOH 1.5 M; soaking in KOH solution for 1 min
4: CS-HEC-C	CS (6 %) + nHA (1.5 %) + HEC (9 %)	Citric acid (20 %w); incubation for 20 min at 165 °C

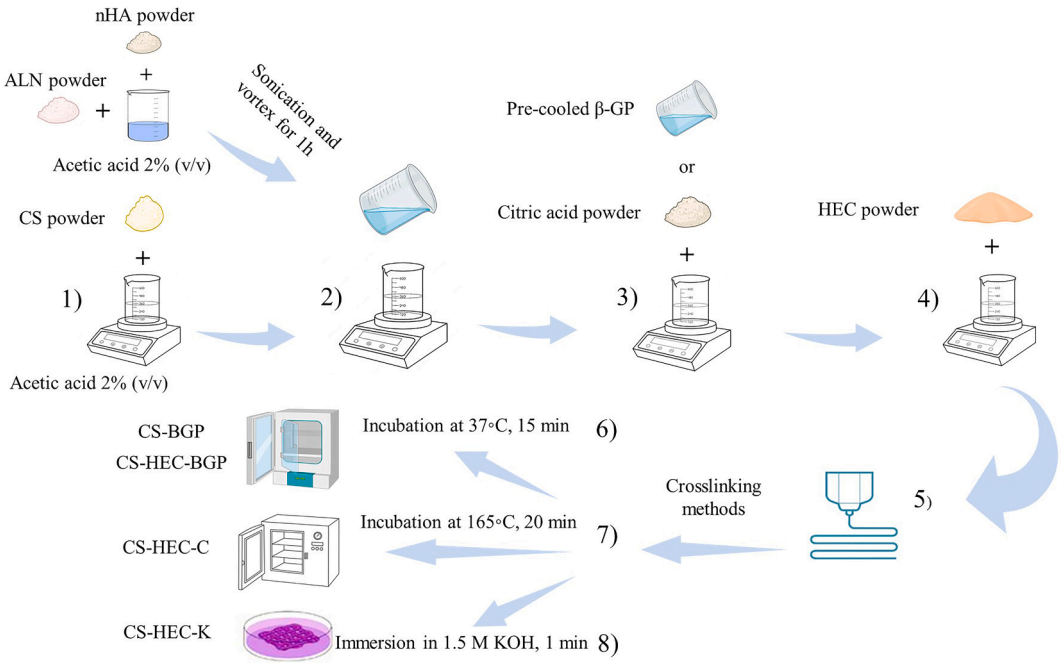

Fig. 1. Schematic representation of hydrogels preparation. Numbers represent different steps of procedures. Ink 1: CS-BGP: at step 3, the addition of B-GP followed by steps 5 and 6 resulted in CS-BGP ink formulation. Ink 2:CS-HEC-BGP: at step 3, addition of β-GP followed by steps 4, 5 and 6 resulted in CS-HEC-BGP formulation. Ink 3: CS-HEC-K: removing step 3, followed by steps 4, 5, and 8 resulted in CS-HEC-K formulation. Ink 4: CS-HEC-C: at step 3, adding citric acid followed by steps 4, 5, and 7 resulted in CS-HEC-C formulation.

with a measuring gap of 100 μm, using a parallel plate geometry of the 8 mm size. 100 μl of the sample was loaded, and after setting the trimming gap, the excess hydrogel outside of the geometry was discarded. Each sample was used for only one test with three replicates. Oil was placed around the sample to avoid dehydration and drying.

Viscosity curves were determined by performing a logarithmic shear rate sweep ($0.01-300\ s^{-1}$). The strain sweep test was done for the strain in the range of 1–1000 % and at the angular frequency of 10 rad/s. Based on the detected linear regime, the strain of 1 % was selected for subsequent sweeps. Afterwards, frequency sweeps were done at 1 % strain with an angular frequency between 1 and 100 rad/s. The angular frequency of 10 rad/s was chosen for time sweep measurements, based on the linear regime. The storage modulus recovery was determined using an experiment with three phases. In phase 1 materials were exposed to a constant shear strain at 1 % for 300 s. In phase 2, 30 s of high shear strain (1000 % for CS-HEC-C and 3000 % for CS-HEC-K sample (inks before crosslinking), application of 1000 % shear strain was not enough for breaking CS-HEC-K sample) was applied to induce inks break; and finally, in phase 3 materials were exposed to another constant shear strain at 1 % for 2 min. The percentage of recovery was defined as:

(**Recovered storage modulus** / **Initial storage modulus**) × **100**.

2.5. Characterization of the scaffolds

2.5.1. Fourier transform infrared spectroscopy (FT-IR)

FT-IR spectra of each scaffold type ($n = 3$) were analyzed using a spectrophotometer (Nicolet Nexus FTIR 670, Thermo Electron, Waltham, MA). Prior to measurement, the samples were freeze-dried (CHRIST, Germany), grained and compressed into pellets.

2.5.2. Degradation test

To determine the degradation rate of CS-HEC-K and CS-HEC-C in PBS solution, the printed and crosslinked scaffolds were immersed and incubated in 2 ml of PBS in 6 well plates. After equilibrating in PBS for 2 h, scaffolds in triplicates were weighed (W_0). Their degradation rate was monitored for 25 days at 37 °C in PBS, with measuring time points on day 1, 2, 3, 4, 5, 10, 15, 20, and 25. At each time point PBS was removed from the plates and scaffolds were weighed (W_t) (in wet form). Afterwards, 2 ml of fresh PBS was added to each well and the procedure was repeated at the following time point. The percentage of degradation (mass loss) was calculated using the following formula (Dong, Wang, Zhao, Zhu, & Yu, 2017):

$$Degradation\ ratio\ (\%) = (W_0 - W_t)/W_0 \times 100$$

2.5.3. Scanning electron microscopy (SEM)

For SEM analysis, the scaffolds were fixed in 4 % paraformaldehyde for 20 min and stored in PBS solution at 4 °C. The samples were then washed with demineralized water and dried under ambient conditions. The scaffolds ($n = 2$ per group) were mounted on an Al stub and examined by SEM without further sample preparation using a FEI (Hilsboro, OR, United States) Quanta 400 FEG at 1.0 kV accelerating voltage under high vacuum conditions.

2.6. Mechanical properties of the scaffolds

2.6.1. Compression test

Static compression test was done for molded CS-BGP after crosslinking, printed CS-HEC-K, and CS-HEC-C samples (after crosslinking) using a TA Rheometer (DHR3, TA Instruments, USA) with parallel plate geometry. Round samples of 8 mm radius were cut with a sharp plunger at different spots of printed scaffolds. Before starting the experiment, the samples were placed at the center of the bottom plate using tweezers. Prior to measurement initialization, the upper plate of the rheometer was manually driven to get into contact with the scaffolds (0 N axial force) and the sample was compressed at a speed of 1 μm/s till the machine reached to highest axial force (50 N). The initial compressive modulus was calculated by using the formula: $\Delta\sigma/\Delta\varepsilon$ for the initial linear part of the stress (σ) vs. strain (ε) plot, where the strain is $\Delta L/L_0$, and L is a measuring gap.

2.7. Drug release assay

ALN concentration was examined with the use of an OPA test. OPA solution was prepared as described before (Church, Porter, Catignani, & Swaisgood, 1985). In brief, 50 mg of OPA was solved in 5 ml pure ethanol, then 250 μl of 2-mercaptoethanol was added and the volume was adjusted to 50 ml using 0.05 M NaOH (Al Deeb, Hamdan, & Al Najjar, 2004). 3D printed scaffolds were incubated in PBS in 12 well plates at 37 °C. To each sample, 1 ml of sterile PBS was added. 500 μl of supernatant was taken from each well at defined time points (1, 3, 5,7, 11, 15, 18, 21, 25, 30, 40, and, 50 days), and replaced with 500 μl fresh PBS. An equal volume of OPA was added and measured at excitation and emission wavelengths of 340 and 455 nm, respectively (using Synergy H4 Hybrid Reader, BioTec, USA). For each ink, drug-free scaffolds were considered as a negative control. A back calculation was used to determine drug release in each time point; since 50 % (v/v) PBS was not refreshed and thus contained drug that was already detected before (Włodarczyk-Biegun et al., 2014). The equation used for the calculation of release was: $T_n = t_n - 0.5\ t_{n-1}$, where T_n is the corrected amount of drug release between time point n and $n-1$, and t_n is the amount of degradation in whole sample at time point n.

2.8. Cell culture

In this study, three cell lines were used: Ad-MSCs (passage 6), MG-63, and RAW 264.7. Ad-MSCs were derived from human adipose tissue, as previously described (Ahmadian kia et al., 2011). The adipose tissue aspirates were received in accordance with the ethical standards of the local ethical committee. MG-63 and RAW 264.7 cells were purchased from the Iranian Biological Resource Center. DMEM containing 1 g/l glucose (low glucose) supplemented with 10 % FBS and 1 % penicillin/streptomycin was used for Ad-MSCs culture. DMEM containing 4.5 g/l glucose (high glucose) supplemented with 10 % FBS and 1 % penicillin/streptomycin was used for MG-63 and RAW 264.7 cell lines. Cells were cultured at 37 °C in the incubator with 5 % CO_2, and the media were refreshed every 3 days. Cells were passaged or used for seeding after reaching 70 % confluency.

2.8.1. Scaffolds sterilization

For sterilization, the CS-HEC-K scaffolds were soaked in 70 % filtered ethanol for 1 h followed by 30 min exposure to UV. The CS-HEC-C were sterilized in an autoclave at 121 °C, and 20 psi pressure, for 20 min.

2.8.2. Cytotoxicity and proliferation assay for CS-BGP formulation

CS-BGP was the only formulation with the capacity of cell encapsulation, because the crosslinking procedure with β-GP was not harmful for cell viability. Therefore, the viability and proliferation were examined only for this ink. In short, the ink was mixed with Ad-MSCs at 10^6 cells /ml concentration and printed. On days 0, 1, and 7 after printing, live/dead assay was performed. In this way, the cell viability under shear stress that is normally applied during 3D bioprinting could also be tested. Staining protocol with fluorescein diacetate (FDA) to detect live cells and propidium iodide (PI) to detect dead cells, was used as follows. Stock solutions of PI (2 mg/ml) and FDA (5 mg/ml) were prepared in PBS and acetone, respectively. 8 μl FDA stock solution and 50 μl PI stock solution were diluted in 5 ml PBS to make a working solution. Then 300 μl of the working solution was added to each well containing the printed scaffold, incubated at room temperature for 5 min, and evaluated by fluorescence microscopy (Nikon ECLIPSE, Ti-S, USA). If necessary, the background was subtracted, and brightness and contrast were adjusted.

2.8.3. Cytotoxicity evaluation of CS-HEC-K and CS-HEC-C by alamarBlue assay

Ad-MSCs at the density of 16,000 cells/cm^2 were seeded in 24 well plates, and incubated at 37 °C with 5 % CO_2 overnight, to reach 60–70 % confluency. After 3 times washing of the sterile scaffolds with PBS, the scaffolds were gently inserted into each well, on top of the cells grown in monolayer. After 1, 3, and 5 days of incubation, cell proliferation was measured by alamarBlue assay. The percentage of alamarBlue reduction was estimated by fluorescence analysis at 530 nm excitation and 590 nm emission wavelengths (Synergy H4 Hybrid Reader, BioTec, USA).

2.8.4. Cell attachment assay for CS-HEC-K and CS-HEC-C formulations

The preliminary assessment of cell attachment to the original CS-HEC-K and CS-HEC-C printed scaffolds showed poor results. To improve the attachment, scaffolds were coated by soaking for 1 h in a sterile solution of: 1) poly-D-lysine (PDL 0.5 and 0.1 mg/ml), 1 h at 37 °C 2) PDL (0.5 mg/ml)/collagen (8 mg/ml) for overnight at 37 °C, 3) 2 % autoclaved gelatin solution for overnight at 37 °C, 4) CS (1 %)/collagen (8 mg/ml) for overnight at 37 °C, 5) Matrigel for 30 min at 37 °C, and 6) gelatin/EDC/NHS. Adding EDC/NHS to gelatin is based on a protocol which is described before (Hermanson, 2013). Briefly, 4 % gelatin was prepared in 0.1 M MES buffer, then EDC and NHS were added to the gelatin solution and the final concentrations of EDC and NHS equaled 100 mM and 50 mM, respectively to induce gelation of gelatin at 37 °C for 1 h. They were then washed 3 times with PBS and transferred to the agarose-treated or non-adherent 24 well plates. A suspension of cells, (Ad-MSC or MG-63) was prepared in 200 μl media and seeded onto the scaffolds at a density of 100,000 cells/cm^2. After pre-incubation for 2 h, 500 μl fresh medium was gently added. After 24 h incubation at 37 °C and 5 % CO_2, the cell attachment and viability wereevaluated using the live/dead assay as described above (Ragetly, Griffon, & Chung, 2010).

2.9. In vitro osteoclastogenesis assay for CS-HEC-K and CS-HEC-C formulations

Osteoclasts were differentiated from mouse monocytes, RAW 264.7 cell line. The RAW 264.7 cells were seeded at a density of 6×10^5 cells/cm^2 in 6 well plates. To elicit osteoclastic differentiation of RAW 264.7 monocyte-like cells, 50 ng/ml of RANKL was used in differentiation medium. Both RANKL negative and RANKL positive groups were considered. RANKL negative groups included scaffold-free wells (untreated) and wells containing CS-HEC-K or CS-HEC-C scaffolds with RANKL-free media. RANKL positive groups included scaffold-free wells (positive control) and wells containing CS-HEC-K or CS-HEC-C scaffolds with differentiation media. After overnight incubation of the cells, the printed scaffolds (CS-HEC-K and CS-HEC-C) were inserted into the wells. Both groups were incubated for 7 days to allow the drug release. Afterwards, the scaffolds were removed and the cells were used for total RNA extraction and qRT-PCR analysis.

2.9.1. RNA extraction, quantification, and reverse transcription

Total RNA was extracted using phenol/chloroform mixture according to the manufacturer's instructions (Riz Molecule Dana, Iran), and dissolved in diethyl pyrocarbonate (DEPC) treated water, pH 7.4. Qualitative and quantitative assessments were done using agarose gel electrophoresis and absorbance measurement at 260 nm, respectively. RNA was treated with DNase I (Fermentas) for 30 min at 37 °C followed by enzyme inactivation with 50 mM ethylenediaminetetraacetic acid (EDTA) at 65 °C to remove genomic DNA residues. Reverse transcription was carried out according to manufacturer's instructions (SuperScript First Strand Kit, Invitrogen) using oligo-dT, at 42 °C for 60 min, followed by incubation at 70 °C for 5 min.

2.9.2. qRT-PCR

The PCR primers (Table 2) were ordered from Metabion (Germany) to verify the expression of *Cathepsin K*, as a specific marker for osteoclasts, and *β-Actin*, as a housekeeping gene (Stephens, Stephens, & Morrison, 2011). The parameters of the primers were assessed by primer-BLAST (https://www.ncbi.nlm.nih.gov/tools/primer-blast/) search tool. SYBR green real-time PCR was performed using iCycler iQ Real-Time PCR Detection System and SYBR green super-mix with 10 μM

Table 2
Primer sequences for qRT-PCR.

Target gene	Forward (5′–3′)/Tm	Reverse (5′–3′)/Tm	Product size (bp)
ACTB	CTCTGGCTCCTAGCACCATGAAGA/64.31 °C	GTAAAACGCAGCTCAGTAACAGTCCG/ 63.77 °C (Nishio et al., 2016)	200
CTSK	CAGCAGAGGTGTGTACTATG/55.30 °C	GCGTTGTTCTTATTCCGAG/57.56 °C (Robinson et al., 2021)	174

primers. The reaction was performed for 35 cycles in the following conditions: 95 °C for 20 s, annealing at 59 °C for 20 s, and 40 s extension at 72 °C.

2.9.3. Statistical analysis of ΔΔCT comparative gene expression

The PCR efficiency was measured using web-based LinRegPCR (https://www.gear-genomics.com/rdml-tools/linregpcr.html) (Untergasser, Ruijter, Benes, & van den Hoff, 2021). The method of Livak and Schmittgen was applied to determine the comparative expression levels between the samples relative to the control (Livak & Schmittgen, 2001). To examine the osteoclast differentiation induced by RANKL, the amplification threshold cycle value (CT) from the RANKL treated sample was subtracted from the untreated well cycle values ($\Delta CT = CT_{untreated} - CT_{RANKL}$). Osteoclast marker expression was normalized to the respective *β-Actin* and expressed as the relative fold increase over the control using $2^{\Delta\Delta CT}$ (Ratio $= 2^{(\Delta CT\ RANKL\ -\Delta CT\ \beta\text{-}Actin)}$) (Granfar, Day, Kim, & Morrison, 2005).

2.10. Statistical analysis

All data were expressed as mean values ± SD. Statistical significance of differences was determined by one-way ANOVA; differences were considered statistically significant at $p < 0.05$, unless it is stated differently.

3. Results and discussion

3.1. 3D printing and crosslinking methods

The aim of this study was to develop a printable formulation, containing ALN as a bioactive drug, for future applications in osteoporotic bone healing. Therefore, the proposed formulations were tested with regards to their printability. For each ink formulation, the optimal extrusion pressure, printing speed, and needle height were determined. The CS-BGP ink formulation containing both 3 % w/v and 6 % w/v CS did not provide a continuous filament printing (Fig. 2a,c,d,f). However, after addition of 8 % w/v CS, the continuous filament was obtained (Fig. 2g and i). For long-term stabilization, the scaffolds printed with CS-BGP were incubated at 37 °C for 15 min. After crosslinking, all the scaffolds were easy to handle (i.e., move with the spatula), yet they revealed poor shape fidelity as observed by the closing of the pores (space between printed filaments) in the printed grid-like structure (Fig. 2c,f,i). We assigned this observation to the relaxation of the printed strands before the crosslinking process could be finalized. These results are corroborated by the report of Ku *et al.* as their CS/BGP (1.67 % w/v chitosan and 56 % w/v β-BG) formulation did not present enough rigidity to support the building of multilayer-scaffold during 3D printing (Ku et al., 2020).

To increase the shape fidelity, HEC at percentage of 9 % w/v was added to the CS-BGP ink (formulation: CS-HEC-BGP). 3 % w/v CS with 9 % w/v HEC was successfully printed with high shape fidelity. 6 % w/v

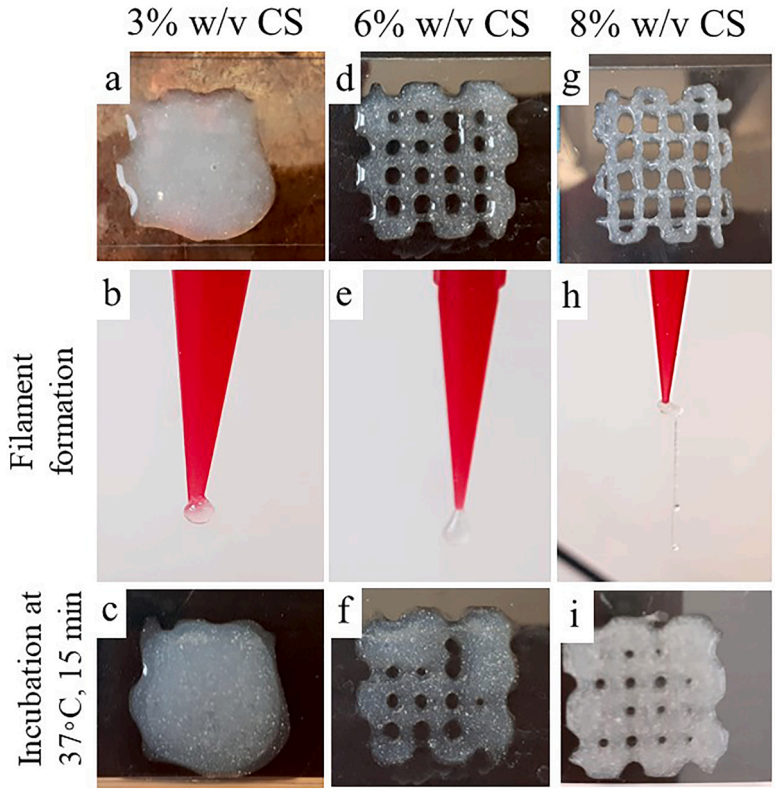

Fig. 2. Printability of CS-based inks containing different amounts of CS: a: 3 % w/v. d: 6 % w/v. g: 8 % w/v. The filament formation using inks with different CS content: b: 3 % w/v. e: 6 % w/v. h: 8 % w/v. Shape fidelity and stability of the scaffolds with different content of CS, containing β-GP as a crosslinker, after incubation at 37 °C for 15 min. c: 3 % w/v. f: 6 % w/v. i: 8 % w/v.

and 8 % w/v CS with the addition of 9 % w/v HEC could not be extruded due to high viscosity. As the percentage of CS increased, the percentage of HEC was decreased to allow material extrusion as both compounds contributed to increased viscosity. The final optimized formulation of CS-HEC-BGP (3 % w/v CS) allowed to print the scaffold with at least 10 layers with no rapid relaxation, and with high shape fidelity. However, after incubation in culture medium, similar to the CS-BGP ink, rapid degradation was observed (within 1 h) (Fig. 2 in SI).

To improve the stability of the printed scaffolds, β-GP as a crosslinker was removed and two other crosslinking approaches, i.e., use of KOH (1) and citric acid (2) were tested to reach printable scaffolds with desired stability. β-GP was kept as a crosslinker in CS-BGP formulation.

(1) The formulation abbreviated as CS-HEC-K, composed of CS (6 % w/v), nHA (1.5 % w/v), and HEC (6 % w/v) was crosslinked using KOH after printing. Briefly, the scaffolds were crosslinked by immersing in 1.5 M KOH solution for 1 min at room temperature. The crosslinking process occurred rapidly, as confirmed by the color of the scaffolds turning turbid white (Fig. 3a–d). The video of printing and crosslinking the CS-HEC-K can be viewed in SI2.
(2) Citric acid (20 % w/w) was added instead of β-GP to the formulation containing CS (6 % w/v), nHA (1.5 % w/v), and HEC (9 % w/v). The content of CS was adjusted to 6 % w/v, as after the addition of the citric acid the viscosity of initial CS-HEC formulation with 3 % w/v HEC was decreased. The crosslinking occurred via high-temperature exposure (165 °C, 20 min) and the scaffold got dried after heating. Heating up resulted also in color change from white before crosslinking to yellowish brown after high-temperature exposure. The images of 3D printed CS-HEC-C showed the highest accuracy (Fig. 3e and f). The video showing the printing process of CS-HEC-C is presented in SI3.

The light microscopy images of the printed scaffolds showed that CS-HEC-C filaments were smoother than CS-HEC-K-based ones (Fig. 3 in SI). Therefore, we found this formulation as the best printable one. All formulations with their printability features are listed in Table 3.

3.2. SEM analysis

The shape and surface morphology of CS-HEC-K and CS-HEC-C printed scaffolds were investigated using SEM imaging. Fig. 4 shows the characteristic surface features of the scaffolds at different magnifications. SEM micrographs showed that strands from different layers can be separated and inks can provide angles on a mesh structure. There is no evidence of material flow in the corners for both scaffold types. Roughness can be detected on the filaments printed in both cases. The CS-HEC-C provided thinner strands and higher resolution that can be considered as the best approach.

Table 3
Printability features of the four developed formulations.

Formulation	Printability	Shape fidelity	Stability	Filament formation
1: CS-BGP	No	No	No	Yes
2:CS-HEC-BGP	Yes	Yes	No	Yes
3: CS-HEC-K	Yes	Yes	Yes	Yes
4: CS-HEC-C	Yes	Yes	Yes	Yes

3.3. Rheological properties of inks

The rheological properties of the materials determine the suitability of the inks for 3D (bio)printing. CS-BGP, CS-HEC-K, and CS-HEC-C were tested for this purpose (see Figs. 5 and 7c–e). For all samples, the tests were applied before crosslinking. It means that the tests for CS-BGP and CS-HEC-C were done before heating, and for the CS-HEC-K, before soaking in KOH solution. The desired rheological properties for (bio)ink formulations include (1) proper viscosity to support shape fidelity after printing, (2) shear-thinning properties to facilitate extrusion, (3) adequate storage modulus recovery, and/or (4) fast gelling kinetics (Hölzl et al., 2016; Ozbolat, Moncal, & Gudapati, 2017). The results of the viscosity measurements showed that all ink formulations exhibited a shear-thinning behavior (Fig. 5a). Shear-thinning property (decrease in viscosity at increasing shear rates) is essential for facilitated extrusion. For good extrudability, the material must flow through the nozzle (increased shear) and needs to retain high viscosity just after injection (no shear) in order to maintain the design at fidelity of the printed structure. The shear-thinning behavior of CS and CS-BGP formulation has been proved by several studies (Rahimnejad, Adoungotchodo, Demarquette, & Lerouge, 2022; Rahimnejad, Labonté-Dupuis, Demarquette, & Lerouge, 2020; Wu, Therriault, & Heuzey, 2018). Based on the data reported by Maturavongsadit *et al.* adding HEC at low percentages (< 1 % w/v) did not alter the shear-thinning property of CS

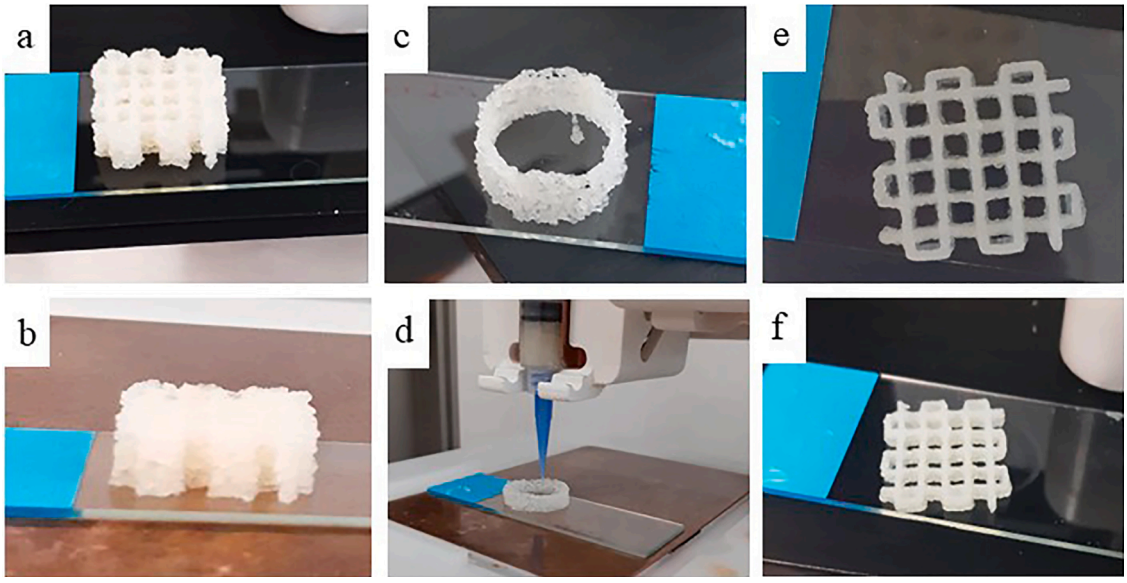

Fig. 3. Images of 3D printed scaffolds with CS-HEC-K ink: cubic shape, 20 layers a: top view, b: side view; round shape, 10 layers c: top view, d: side view. CS-HEC-C ink: cubic shape, 10 layers e: top view. f: side view.

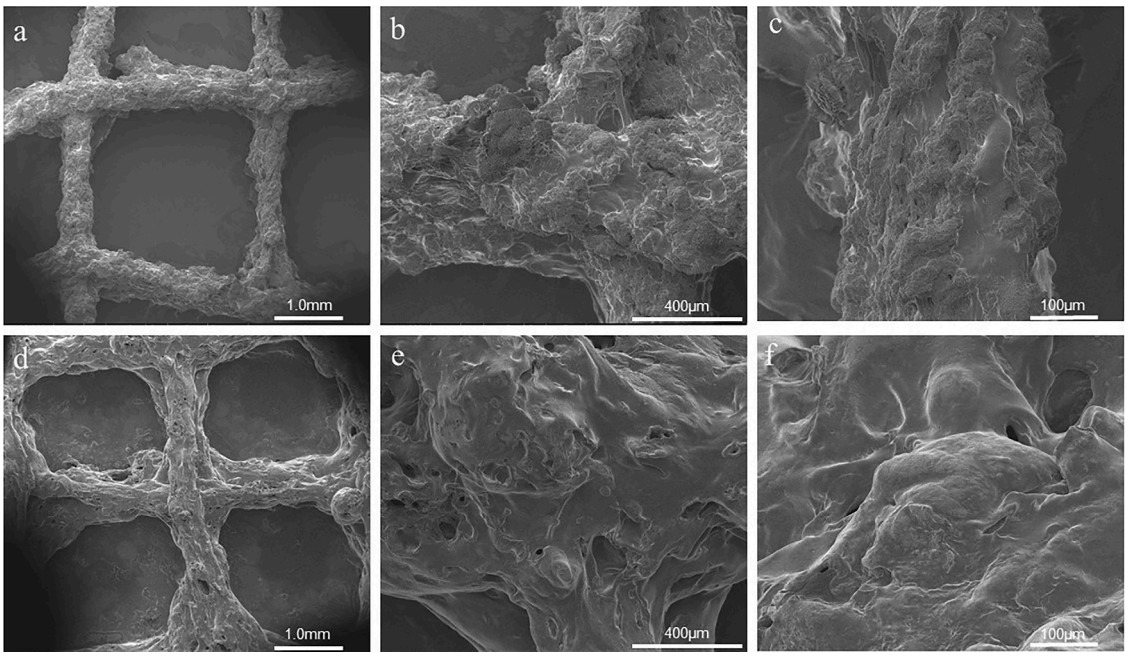

Fig. 4. SEM images of 3D printed scaffolds at different magnifications. a–c: CS-HEC-K formulation; d–f: CS-HEC-C formulation. a and d show scaffolds at 50x magnification, b and e: 200x magnification, c and f: 500x magnification.

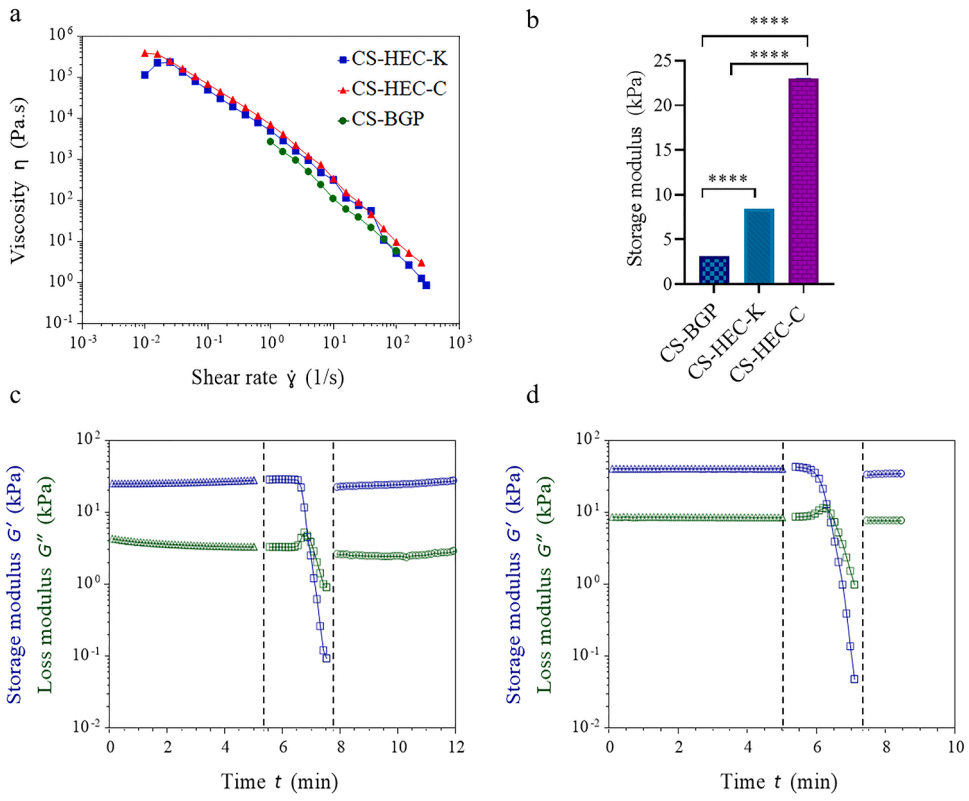

Fig. 5. Rheological properties of CS-BGP, CS-HEC-K and CS-HEC-C inks before crosslinking. a: Viscosity curves of inks determined at a shear rate ranging from 10^{-2} to 10^{2} s^{-1}. b: Storage modulus of three tested inks, $^{****}p < 0.0001$. c: Storage modulus recovery of CS-HEC-K after undergoing 3000 % strain. d: Storage modulus recovery of CS-HEC-C after undergoing 1000 % strain.

(Maturavongsadit, Narayanan, Chansoria, Shirwaiker, & Benhabbour, 2021). Our results proved the shear-thinning properties of CS/HEC ink in the presence of HEC up to 9 % w/v.

The rheology features of inks before crosslinking were determined by measuring the storage modulus (G′) and loss modulus (G″). All 3 inks revealed solid-like behavior ($G' > G''$). The highest storage modulus was recorded for CS-HEC-C ink (G′ of CS-HEC-C > CS-HEC-K > CS-BGP) (Fig. 5b). The polymer with the highest storage modulus can be expected to be the most stable after printing (Kimbell & Azad, 2021). The CS-BGP ink had the lowest storage modulus and led to rapid relaxation during

printing (see Section 3.1). The rheology results for sample replicates can be found in SI.

Testing the consecutive steps of breaking and recovery of inks was performed to imitate the printing process. Applying high strain during printing can damage the hydrogel, possibly affecting its printability potential. The storage modulus recovery of inks was determined as an indicator of the ability to reach the original material stiffness, before the breakage. Based on the results, after applying a high shear strain, both CS-HEC-C and CS-HEC-K exhibited a very similar recovered modulus to the initial one, which is desired for 3D printing. The recovery percentage for CS-HEC-C and CS-HEC-K was 84.24 ± 1.2 % and 97.02 ± 5.9 %, respectively (Fig. 5c and d).

3.4. Interactions between the components of the inks and crosslinking mechanisms

Fig. 6 illustrates the expected interactions between the different components of the hydrogels and anticipated crosslinking mechanisms for three studied inks: CS-BGP, CS-HES-K and CS-HEC-C. The interaction of CS and β-GP depends on several factors, with the most prominent electrostatic interaction between positive groups of CS (amine groups) and the negative charge of β-GP (phosphate groups) (Rahmanian-Devin, Baradaran Rahimi, & Askari, 2021). In addition, increasing the pH of CS solution by β-GP involves hydrogen bonds and hydrophobic effects, leading to CS precipitation. β-GP can induce gelation by increasing the temperature above 37 °C (Fig. 6a) (Rahmanian-Devin et al., 2021).

All the developed inks contained nHA. We expect hydroxyl ions on the surface of nHA to interact with the amino and hydroxyl ions of chitosan by the formation of hydrogen bonds (Fig. 6b) (Xianmiao et al., 2009). Further, we expect ALN, as a bisphosphonate, to interact with nHA. ALN has two phosphate groups with strong affinity to calcium (Ca^{2+}) in nHA, which inhibits the nHA crystal growth (Gao et al., 2017). In fact, by a bidentate chelation of deprotonated oxygen atoms, the two phosphonate groups can interact with calcium atoms on the nHA surface. Some studies also indicated that the nitrogen groups of ALN can bind to the hydroxyl group on the nHA surface forming N–H–O hydrogen bonds (Bigi & Boanini, 2018).

In this study, HEC was used as a thickening agent to improve the printability of the CS-containing inks. Based on the previous reports (Maturavongsadit, Paravyan, Shrivastava, & Benhabbour, 2020) the chemical crosslinking between CS and HEC can happen via Schiff-base linkages. Maturavongsadit *et al.* reported that the reactive glyoxal molecules from HEC were required to promote crosslinking of the amine groups in the CS network and form hydrogel systems. They showed that the presence of glyoxal group in HEC can be used as a secondary crosslinker to promote rapid gelling of the CS system (Maturavongsadit et al., 2020). However, the HEC used in our study does not have glyoxal groups and therefore we do not expect chemical bonds between CS and HEC.

To improve printability and stability of the scaffolds, citric acid was added. Citric acid can work as a linker between different polymer chains which was reported for CS–CS (Zhuang, Zhi, Du, & Yuan, 2020), CS–HEC (Uyanga & Daoud, 2021), and HEC–HEC (Marani, Bloisi, & Petri, 2015). The CS–CS can be crosslinked with citric acid intermolecularly (crosslinking of two different CS chains) or intramolecularly (cross-links within same CS chain). The protonated N atoms of CS are easily attacked by a lone pair owned by the -OH group of citric acid (Fig. 6c) (Lusiana, Siswanta, & Mudasir, 2016; Zhuang et al., 2020). Citric acid also has the ability to crosslink the hydroxyl groups of cellulose and its derivatives such as HEC via an esterification mechanism. The process happens under the esterification reaction which needs a high temperature: 165 °C, 20 min (Marani et al., 2015; Raucci et al., 2015). In this mechanism, carboxylic acid anhydride is formed by intramolecular dehydration and then reacts with the hydroxyl group of the polymer to form an ester group (Fig. 6d) (Ayouch et al., 2021). Crosslinking mechanism between CS and HEC in the presence of citric acid is also an esterification process. The $COO^-$and OH groups of citric acid crosslink through ester formation leading to the development of the hydrogel (Fig. 6e) (Uyanga & Daoud, 2021). We anticipated that a Maillard reaction occurred between CS and citric acid during applying high temperatures (Petitjean, Aussant, Vergara, & Isasi, 2020; Zarandona, Minh, Trung, de la Caba, & Guerrero, 2021). At higher temperatures, dry heat-produced chromophores in CS may be related to interchain crosslink formation involving the NH_2 groups (Lim, Khor, & Ling, 1999; Yang, Zhao, Liu, Ding, & Gu, 2007). Therefore, the color of CS-HEC-C ink got yellowish brown after heating.

The addition of KOH (1.5 M) was also used as an alternative crosslinking mechanism. It changes the pH of the scaffolds rapidly, leading to deprotonation of amine groups of CS and causing physical crosslinking and self-assembling (Yang, Chen, Murray, & Zhang, 2020). This approach is compatible with Bergonzy *et al.* report. They used 1.5 M KOH as a strong base for CS-based scaffold crosslinking (Bergonzi et al.,

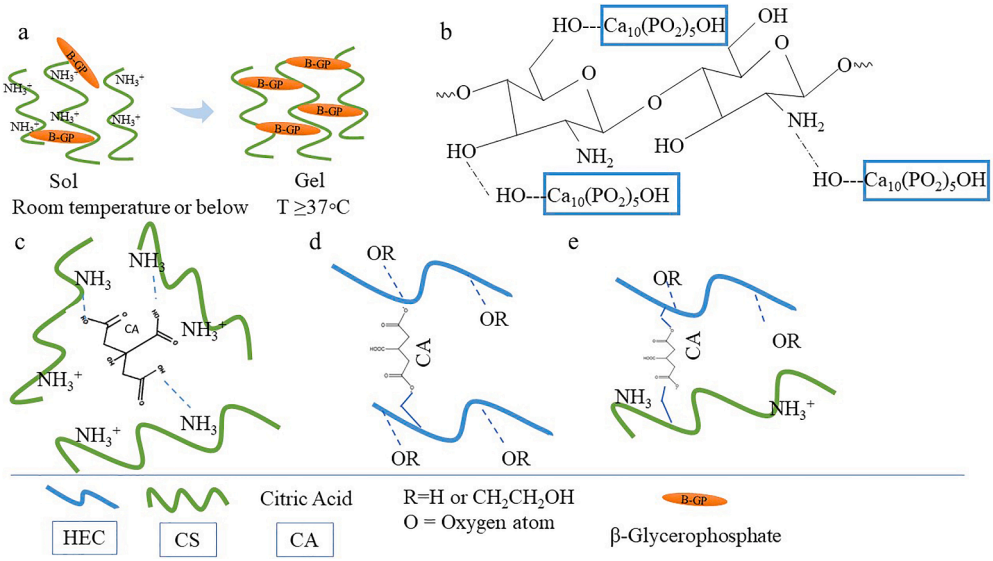

Fig. 6. Chemical interactions between the compunds of the developed inks. a: Schematic view of chemical interactions between CS and β-GP in CS-BGP and CS-HEC-BGP formulations. b: Chemical interactions between CS and nHA. c: CS-CS chemichal crosslinking via citric acid in CS-HEC-K and CS-HEC-C inks. d: HEC-HEC chemical crosslinking via citric acid in CS-HEC-K and CS-HEC-C inks. e: CS-HEC chemical crosslinking via citric acid in CS-HEC-K and CS-HEC-C formulations.

2019).

FT-IR and rheology measurements were performed for printable scaffolds before and after crosslinking process to confirm the crosslinking bonds. In CS-HEC-K scaffolds, band I, II, and III shifting appeared which could be assigned to deprotonation of amine groups in CS following their contact with KOH (Fig. 7a). This deprotonation reduced the hydration shell of the amine groups and allowed new hydrogen bonds to form in the CH chains. C═O in the amide group (amide I band) was shifted from 1629 cm^{-1} to 1657 cm^{-1}. NH-bending vibration in the amide group and NH_2 in the amino group were 1558 and 1380 cm^{-1} before crosslinking, respectively. After soaking in KOH, they were shifted from 1558 cm^{-1} to 1574 cm^{-1} and from 1380 cm^{-1} to 1388 cm^{-1} (Fig. 7a) that is similar to a previous report, which used NaOH base for crosslinking CS (Takara, Marchese, & Ochoa, 2015). In the CS-HEC-C formulation, both spectra were generally similar, just the additional peak (ester stretch of the citrate) for the crosslinked scaffolds appeared at 1715.13 cm^{-1} (Fig. 7b), which is confirmed by previous studies (Ayouch et al., 2021; Halpern et al., 2014). Frequency-sweep tests performed for all inks before and after crosslinking (Fig. 7c–e) further corroborated the FT-IR-based indication that all the inks were successfully crosslinked. G′ and G″ values for all 3 inks were significantly increased after the crosslinking process. The highest increase in the G′ value after crosslinking was observed for CS-BGP, while the lowest was related to CS-HEC-K. The final storage moduli after crosslinking for CS-BGP and CS-HEC-C inks were similar.

3.5. Degradation assessment of the printed formulations

In order to examine the biodegradability and stability of the scaffolds in a culture medium, the printed formulations CS-HEC-BGP, CS-HEC-K, and CS-HEC-C were selected for degradation assessment. This would evaluate the applicability of the scaffolds for cell culture and long-term

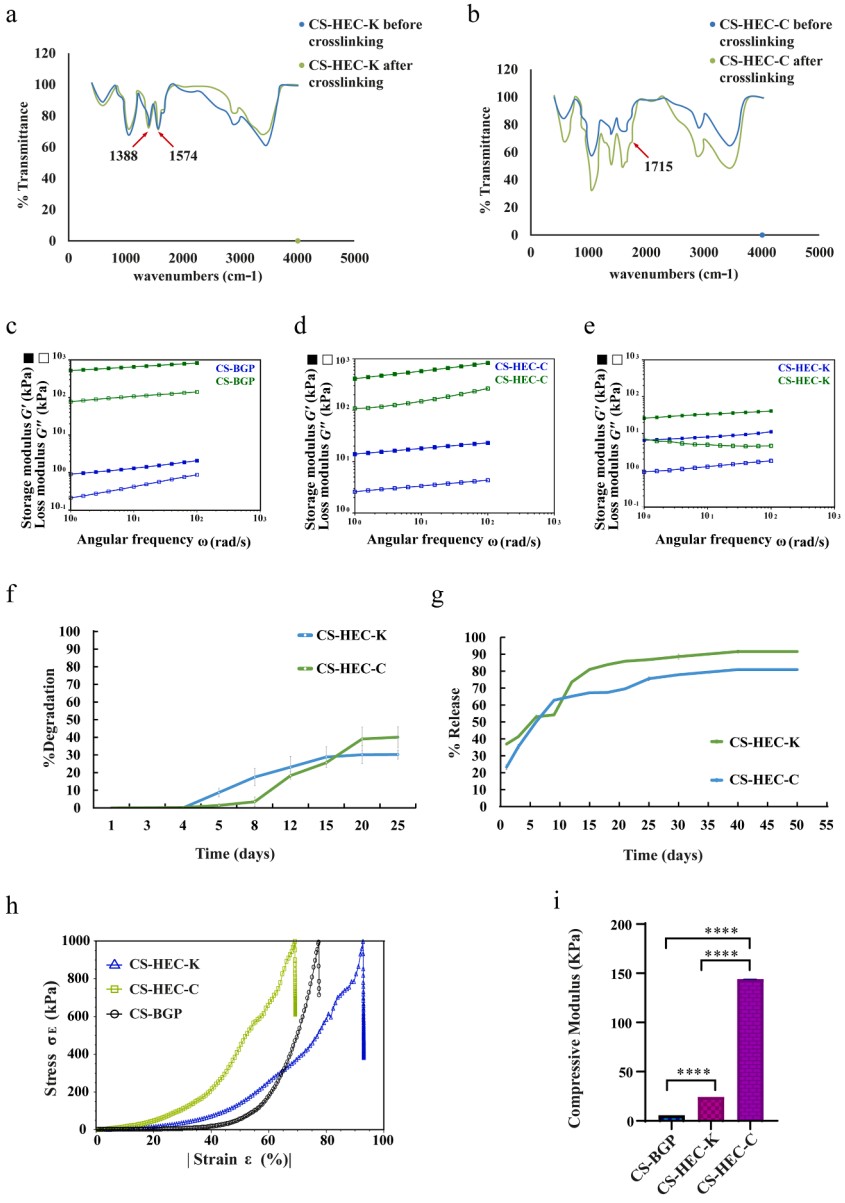

Fig. 7. Scaffolds analysis after crosslinking process: a: FT-IR results for CS-HEC-K formulation before and after crosslinking. b: FT-IR spectra for CS-HEC-C formulation before and after crosslinking. c-e: The storage and loss moduli, G′ and G″ recorded as a function of frequency between 1 and 10^2 rad/s at 1 % strain before (blue) and after (green) crosslinking for c: CS-BGP, d: CH-HEC-C and e: CS-HEC-K. f: *In vitro* degradation percentage of CS-HEC-K and CS-HEC-C in PBS. g: Cumulative release of ALN from CS-HEC-K and CS-HEC-C during 50 days. Values present the means of three replicate ± SD. h: Compressive stress–stain curves of CS-BGP, CS-HEC-K and CS-HEC-C inks, i: Compressive modulus of CS-BGP, CS-HEC-K and CS-HEC-C. ****$p < 0.0001$.

drug release. CS-HEC-BGP formulation showed very fast degradation (less than 1 h) in PBS and medium (see Section 3.1, Fig. 2, SI). Due to very poor stability in the medium, CS-HEC-BGP was not further characterized. The results of *in vitro* degradation for CS-HEC-K and CS-HEC-C proved their high stability in PBS during 25 days. In the first four days, no erosion was detected for both mentioned formulations. The degradation profile of CS-HEC-K formulation increased on the 8th day from 17.44 % to 39 % (Fig. 7f). The degradation rate of CS-HEC-C increased dramatically from 0 % to 25 % on the 15th day and then exhibited a plateau phase. The final degradation rate of CS-HEC-C was higher than that of CS-HEC-K. However, both scaffolds proved to have suitable stability for *in vitro* cytocompatibility assay. The detected degradation of 35–40 % for CS-HEC-K scaffolds during 25 days is close to the data obtained for 3D printed scaffolds made of 10 % CS in another study (Sadeghianmaryan et al., 2020). In addition, the microscopy images of scaffolds during 7 days of incubation at 37 °C were taken and revealed that the scaffolds maintained their initial shape for at least 7 days (Fig. 4 in SI). The results of the degradation studies are an indicator of the material temporal stability, also at an increased temperature.

3.6. Drug release

ALN was added to the CS-HEC-K and CS-HEC-C scaffolds to postpone the reinitiating of osteoclast activity in osteoporotic bones. An initial burst release was measured after 2 h at the levels of 36.96 % and 23.25 % for CS-HEC-K and CS-HEC-C, respectively (see Fig. 7g). This could be ascribed to the escaped free hydrophilic ALN drug from the hydrogel. The cumulative release reached the highest point within the first 25 days of the experiment for both mentioned formulations. In total, after 50 days, 91 % and 80 % of the initial dose of ALN was released from CS-HEC-K and CS-HEC-C, respectively (Fig. 7g). A similar cumulative profile of release was reported for ALN-loaded PLGA nanoparticles in gellan gum (Posadowska et al., 2015). However, their initial burst release was around 4 % during the first 5 days which is lower than our result, and might be due to the presence of PLGA shell. Sustained release behavior for ALN loaded PEG-based hydrogel with 80 % release was also reported during 12 days (Chang et al., 2022), which is significantly shorter than that of our study. ALN release for more than 60 days was also reported from bulk CS/BGP (Nafee, Zewail, & Boraie, 2018). 50 days of ALN release can inhibit the osteoclast activity at the OS defected site and can provide an opportunity for Ad-MSCs to differentiate and start producing natural bone ECM. The time needed for differentiation of Ad-MSCs to osteoblasts, is 14–21 days. Therefore, 50 days of release is sufficient to postpone scaffold degradation by osteoclasts. Despite a fast initial release, both CS-HEC-K and CS-HEC-C systems showed the ability to deliver ALN with constant dosage.

3.7. Compression test

Compression tests were carried out to evaluate the compression modulus of the printed CS-HEC-K and CS-HEC-C and bulk CS-BGP after printing and crosslinking. The stress–strain curves of all the samples showed a linear initial phase (up to 5 % strain for all three inks) which was used for calculation of compression modulus (Fig. 7h). The CS-HEC-C and CS-HEC-K revealed the highest and lowest modulus, respectively. The compressive module of CS-BGP was 5.8 kPa, CS-HEC-K 24.3 kPa, and CS-HEC-C 144 kPa (Fig. 7i). The reported compressive module for CS and CS/gelatin is approximately between the range of 5–200 kPa (Levengood & Zhang, 2014), which is similar to the CS-BGP and CS-HEC-K scaffolds. Various factors including the molecular weight, the percentage of CS, and the degree of scaffold hydration can alter the compressive modulus. Therefore, it is difficult to directly compare the mechanical properties of CS-based hydrogels. The module measured for CS-HEC-C in this study, was the highest. The presence of stem cells and the ECM produced by the cells could further increase the mechanical properties to reach values close to native tissue.

3.8. In vitro cell studies

3.8.1. Cytotoxicity result of CS-BGP

Ad-MSCs were encapsulated in the CS-BGP ink, and the material was extruded and cast. Cell viability was qualitatively evaluated by imaging live and dead cells using FDA/PI staining. Fig. 8 shows the viability of the cells just after printing (day zero) (Fig. 8a), and after 1 and 7 days of incubation (Fig. 8b and c). The results demonstrated high cell viability within the material. Gradual increase in the number of living cells by time reveals that CS-BGP can also support cell proliferation. The CS-BGP was not a printable formulation, however it can be used as an injectable one.

3.8.2. Biocompatibility of CS-HEC-K and CS-HEC-C formulations

The viability of Ad-MSCs was evaluated in contact with CS-HEC-K and CS-HEC-C scaffolds using alamarBlue assay. For this purpose, the scaffolds were inserted on top of the Ad-MSCs cultured in the multi-well plates. Positive control comprised of cells without scaffolds. AlamarBlue is based on the oxidation-reduction capacity of living cells. AlamarBlue or resazurin can be reduced via live cells to the highly fluorescent pink resorufin. The difference in reduction of alamarBlue between positive well (scaffold-free) and test groups (containing printed scaffolds) was considered as an indicator for cell viability/material toxicity. Based on the results, an increase in the cell number was observed for both CS-HEC-K and CS-HEC-C scaffolds. No significant difference was detected between the test groups and control group. Therefore, we concluded that 3D printed scaffolds did not show any cytotoxicity on human Ad-MSCs (Fig. 8d).

3.8.3. Cell attachment on CS-HEC-K and CS-HEC-C formulations

The results of cell attachment to the scaffolds printed with CS-HEC-K and CS-HEC-C inks showed that uncoated scaffolds were inefficient. Not enough cells were detected on the original scaffolds (Fig. 10 in SI). CS is a ligand free for cell attachment and its surface charge can determine the possibility of cell adherence. The charge of CS is highly related to the pH and the type of crosslinker. After addition of KOH to the CS-HEC-K formulation, the CS underwent deprotonation. Therefore, the surface charge of the CS-HEC-K was neutral or slightly negative. In the case of the CS-HEC-C, the citric acid can use amine groups of CS in the crosslinking process and the surface of CS-HEC-C formulation was expected to be neutral (Courtenay et al., 2018; Ferrari, Cirisano, & Morán, 2019). Therefore, poor cell adherence was not surprising. This conclusion can be validated by large number of studies indicating that cell adherence is higher to positively charged surfaces rather than negatively charged ones (Cai et al., 2020; Metwally et al., 2020). To improve cell attachment, different coating layers were assessed. For this porpose, PDL/collagen, gelatin, CS/collagen, Matrigel and gelatin/EDC/NHS as coating layers were tested. PDL/collagen can make a positive surface for cell attachment, adding collagen also provides ligands for cells to be bonded to collagen-binding integrins (Davidenko et al., 2016). For the formulation of CS-HEC-K, we could not use collagen coating, because collagen solution in acetic acid (0.02 % v/v) would dissolve the scaffolds, as the crosslinking with the KOH interaction is reversible. To solve this problem, CS-HEC-K were soaked in gelatin solution at 37 °C overnight. Gelatin provides an ideal surface for cells that express gelatin-binding receptors. The gelatin coated CS-HEC-K showed suitable cell attachment on filaments (Fig. 9a and b). According to the FDA/PI imaging, the CS-HEC-C, coated with PDL/collagen (Fig. 9c and d), CS/collagen (Fig. 9e and f), and gelatin/EDC/NHS (Fig. 9g), showed improved cell attachment with visible living cells (green signal) after 24 h of incubation for both Ad-MSCs and MG-63 cells. Matrigel coated scaffolds showed a high cell attachment; however, after 24 h the thin Matrigel layer together with cells was dissociated from the surface of the scaffolds (Fig. 11 in SI). Because of the dissolution of collagenous coating layers, the proliferation of the cells for more days was not possible and more research on the chemistry of the coating is required.

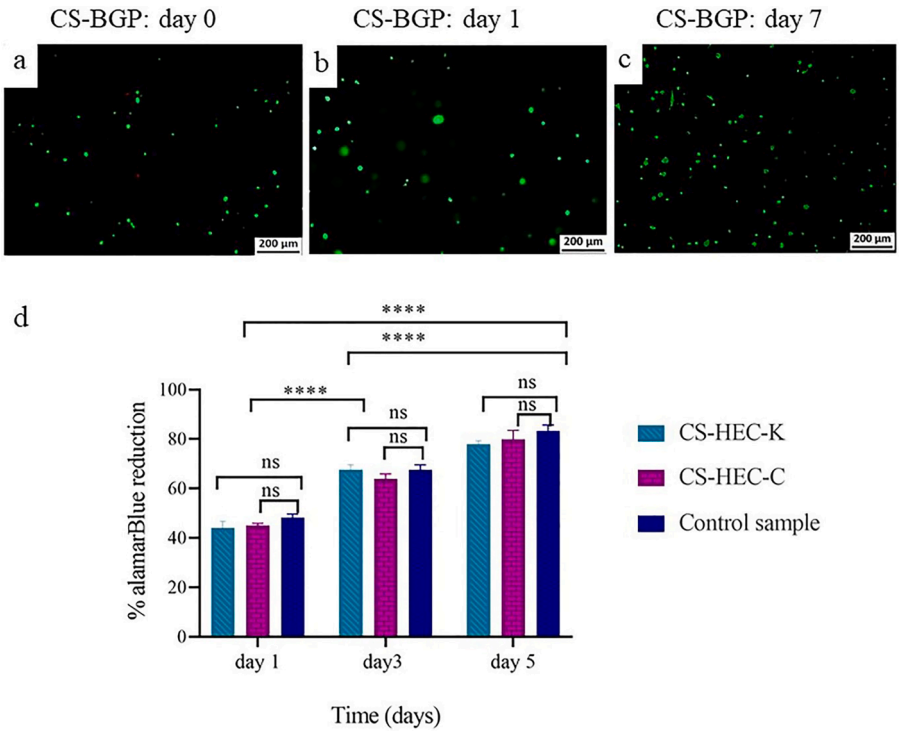

Fig. 8. Live/dead assay for cell-encapsulated 3D printed CS-BGP. a: Day 0, b: day 3, c: day 7, d. AlamarBlue cell viability results of Ad-MSCs in contact with the scaffolds after 1, 3 and 5 days of incubation. Control sample contains cells without any scaffolds on top of that. Values present the means of three replicate ± SD. ANOVA multiple tests: ns: not significant, ****$p < 0.0001$.

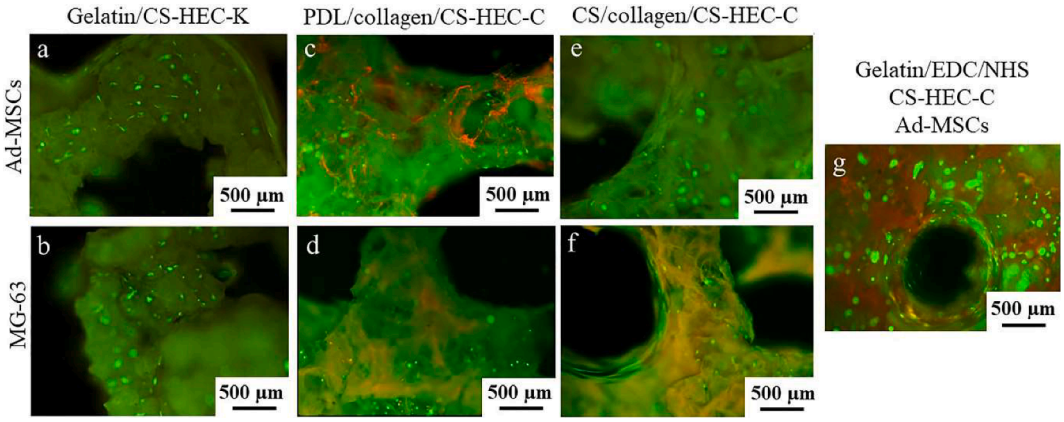

Fig. 9. Fluorescence microscopy images are taken from live/dead assay of Ad-MSCs and MG-63 cells seeded on the CS-HEC-K and CS-HEC-C scaffolds and cultured for 24 h in presense of different coating layeres. Green signals represent the live cells and red signals represent dead cells. The merged images are shown and the scale bar represents 500 µm.

3.9. *In vitro osteoclastogenesis*

The qRT-PCR was used to measure the expression of an osteoclast-specific gene marker *CTSK* (Wilson, Peters, Saftig, & Brömme, 2009). *Cathepsin K*, encoded by *CTSK*, is a distinctive marker in osteoclasts which is responsible for the digestion of type I collagen in osteoclast-mediated bone resorption. RAW 264.7 cells can differentiate to osteoclasts in the presence of RANKL (Collin-Osdoby, Yu, Zheng, & Osdoby, 2003). Osteoclasts differentiated from RAW 264.7 cells represent essential characteristics of osteoclasts, notably the expression of *CTSK* (Cheng et al., 2022). We determined the expression profile of this gene for RANKL negative and RANKL positive groups. The method of Livak and Schmittgen was applied to determine the relative expression levels of the samples in comparison to control gene expression (*ACTB*). Based on the results, the RANKL positive group (scaffold-free) showed the highest relative expression level of *CTSK* gene. There was no *CTSK* expression in RANKL negative groups whether in presence of drug-loaded scaffold or not. This result demonstrated that the ALN-containing scaffold cannot induce *Cathepsin K* production in the absence of RANKL. Simultaneously, the expression of *CTSK* in cells from the CS-HEC-K and CS-HEC-C in the RANKL positive groups was reduced (Fig. 10). Down-regulation of *CTSK* expression was expected due to ALN release. Bisphosphonates can inhibit the osteoclasts via different mechanisms. In the human body, ALN binds to bone mineral, where it is absorbed by mature osteoclasts, inducing osteoclast apoptosis and suppressing bone resorption (Pedersen, Heide-Jørgensen, Sørensen, Prieto-Alhambra, & Ehrenstein, 2019). Another study also suggested that long-term use of ALN can reduce the formation of osteoclast

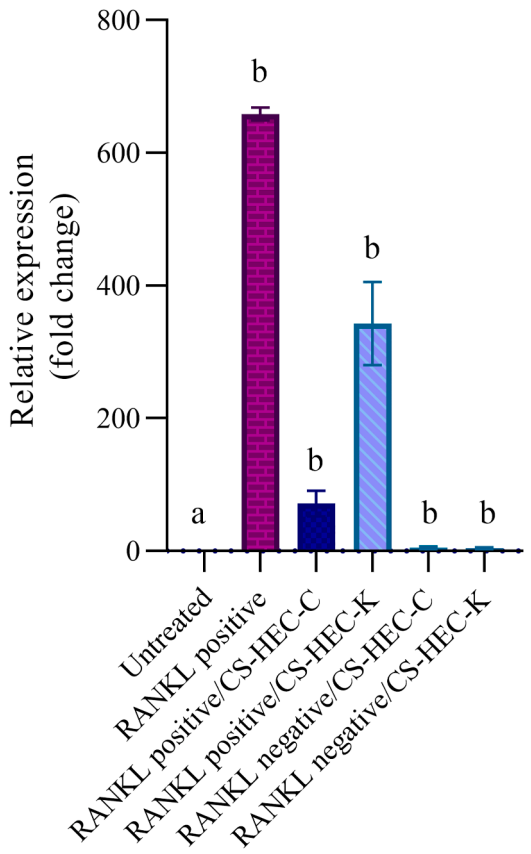

Fig. 10. Graph with relative expression of *CTSK* gene. Fold change in gene expression was evaluated by qRT-PCR, according to the $2^{\Delta\Delta CT}$ method. Untreated represents the scaffold-free well in the RANKL negative group. RANKL positive represents the scaffold-free well in RANKL positive group. Different letters (a,b) denote the statistical difference between untreated (control) and treated samples as determined by pair Student's *t*-test ($p < 0.05$). Values present the means of three replicate ± SD.

precursors. Several studies demonstrated that the low concentration of ALN can inhibit osteoclastogenesis of RAW 264.7 cells *in vitro*, as we observed in our results (Al-Baadani et al., 2022; Kim et al., 2012; Martins, Leyhausen, Volk, & Geurtsen, 2015; Zhang et al., 2013). Moreover, ALN can induce apoptosis in pre-osteoclasts as well as mature osteoclasts (Abe et al., 2012). The gel electrophoresis analysis of total RNA extraction is reported in SI (Fig. 12 in SI).

4. Conclusions

In search for future solutions to improve osteoporosis treatment, in this study, we designed two printable and one injectable CS-based materials with capacity of drug and cell delivery. CS-HEC-K and CS-HEC-C formulations were well printable and biocompatible. The process of synthesis of hydrogels is simple and robust. After coating with different methods, the scaffolds showed improved cell attachment compared to the original ones. Drug-loaded scaffolds exhibited gradual release of ALN during 50 days. The effect of drug-loaded CS-HEC-K and CS-HEC-C on the inhibition of osteoclastogenesis was proved by qRT-PCR. The release of ALN in this period can inhibit osteoclast activity and allow stem cells to regenerate the ECM at the vulnerable site. The proposed injectable hydrogel based on CS and β-GP allowed for cell encapsulation and supported their survival and proliferation. We envision that this formulation can be beneficial as an injectable filler for OS prevention via non-invasive methods.

Funding

J.Z–P. and M.K. W–B. acknowledge financial support from the Polish National Agency for Academic Exchange [NAWA, Polish Returns grant no. PPN/PPO/2019/1/00004/U/0001] and the National Science Centre, Poland (NCN, OPUS grant no. 2020/37/B/ST5/00743]. S.A. acknowledges support from the Silesian University of Technology in the framework of Excellence Initiative - Research University program implemented in 2021 (project no. 32/007/SDU/10-22- 672 04) and support from Ferdowsi University of Mashhad [grant no. 53146].

CRediT authorship contribution statement

Simindokht Afra: Writing – review & editing, Writing – original draft, Visualization, Methodology, Formal analysis, Data curation, Conceptualization. **Marcus Koch:** Writing – review & editing, Formal analysis, Data curation. **Joanna Żur-Pińska:** Writing – review & editing, Visualization, Validation, Supervision, Methodology, Data curation. **Maryam Dolatshahi:** Data curation. **Ahmad Reza Bahrami:** Writing – review & editing, Funding acquisition. **Julien Es Sayed:** Writing – review & editing, Supervision, Methodology. **Ali Moradi:** Writing – review & editing, Conceptualization. **Maryam M. Matin:** Conceptualization, Validation, Writing – review & editing, Supervision, Funding acquisition. **Małgorzata Katarzyna Włodarczyk-Biegun:** Writing – review & editing, Validation, Supervision, Funding acquisition, Conceptualization.

Declaration of competing interest

The authors declare that they have no known competing financial interests or personal relationships that could have appeared to influence the work reported in this paper.

Data availability

Data will be made available on request.

Acknowledgment

We would like to thank Pavan Gudeti, Anna Byczek-Wyrostek, Mohammad Hasan Mollaei, and Lukas Schwab for their valuable support.

Supplementary materials

Supplementary materials associated with this article can be found, in the online version, at doi:10.1016/j.carpta.2023.100418.

References

Abe, K., Yoshimura, Y., Deyama, Y., Kikuiri, T., Hasegawa, T., Tei, K., & Kitagawa, Y. (2012). Effects of bisphosphonates on osteoclastogenesis in RAW264.7 cells. *International Journal of Molecular Medicine, 29*(6), 1007–1015.

Adami, G., Fassio, A., Gatti, D., Viapiana, O., Benini, C., Danila, M. I., & Rossini, M. (2022). Osteoporosis in 10 years time: A glimpse into the future of osteoporosis. *Therapeutic Advances in Musculoskeletal Disease, 14*, Article 1759720x221083541.

Ahmadian kia, N., Bahrami, A. R., Ebrahimi, M., Matin, M. M., Neshati, Z., Almohaddesin, M. R., & Bidurnkhori, H. R. (2011). Comparative analysis of chemokine receptor's expression in mesenchymal stem cells derived from human bone marrow and adipose tissue. *Journal of Molecular Neuroscience, 44*(3), 178–185.

Al-Baadani, M. A., Xu, L., Hii Ru Yie, K., Sun, A., Gao, X., Cai, K., & Ma, P. (2022). In situ preparation of alendronate-loaded ZIF-8 nanoparticles on electrospun nanofibers for accelerating early osteogenesis in osteoporosis. *Materials & Design, 217*, Article 110596.

Al Deeb, S. K., Hamdan, I. I., & Al Najjar, S. M. (2004). Spectroscopic and HPLC methods for the determination of alendronate in tablets and urine. *Talanta, 64*(3), 695–702.

Ayouch, I., Kassem, I., Kassab, Z., Barrak, I., Barhoun, A., Jacquemin, J., & Achaby, M. E. (2021). Crosslinked carboxymethyl cellulose-hydroxyethyl cellulose hydrogel films

for adsorption of cadmium and methylene blue from aqueous solutions. *Surfaces and Interfaces, 24*, Article 101124.
Bellich, B., D'Agostino, I., Semeraro, S., Gamini, A., & Cesàro, A. (2016). The good, the bad and the ugly" of chitosans. *Marine Drugs, 14*(5).
Bergonzi, C., Di Natale, A., Zimetti, F., Marchi, C., Bianchera, A., Bernini, F., & Elviri, L. (2019). Study of 3D-printed chitosan scaffold features after different post-printing gelation processes. *Scientific Reports, 9*(1), 362.
Bigi, A., & Boanini, E. (2018). Calcium phosphates as delivery systems for bisphosphonates. *Journal of Functional Biomaterials, 9*(1).
Bone, H. G., Wagman, R. B., Brandi, M. L., Brown, J. P., Chapurlat, R., Cummings, S. R., & Papapoulos, S. (2017). 10 years of denosumab treatment in postmenopausal women with osteoporosis: Results from the phase 3 randomised FREEDOM trial and open-label extension. *The Lancet Diabetes & Endocrinology, 5*(7), 513–523.
Cai, S., Wu, C., Yang, W., Liang, W., Yu, H., & Liu, L. (2020). Recent advance in surface modification for regulating cell adhesion and behaviors. *The Nanotechnology Reviews, 9*(1), 971–989.
Chang, S., Li, C., Xu, N., Wang, J., Jing, Z., Cai, H., & Wang, X. (2022). A sustained release of alendronate from an injectable tetra-PEG hydrogel for efficient bone repair. *Frontiers in Bioengineering and Biotechnology, 10*.
Cheng, Y., Liu, H., Li, J., Ma, Y., Song, C., Wang, Y., & Zhang, Z. (2022). Evaluation of culture conditions for osteoclastogenesis in RAW264.7 cells. *PloS one, 17*(11), Article e0277871.
Church, F. C., Porter, D. H., Catignani, G. L., & Swaisgood, H. E. (1985). An o-phthalaldehyde spectrophotometric assay for proteinases. *Analytical Biochemistry, 146*(2), 343–348.
Collin-Osdoby, P., Yu, X., Zheng, H., & Osdoby, P. (2003). RANKL-mediated osteoclast formation from murine RAW 264.7 cells. *Methods in Molecular Medicine, 80*, 153–166.
Courtenay, J. C., Deneke, C., Lanzoni, E. M., Costa, C. A., Bae, Y., Scott, J. L., & Sharma, R. I. (2018). Modulating cell response on cellulose surfaces; tunable attachment and scaffold mechanics. *Cellulose (Lond), 25*(2), 925–940.
Davidenko, N., Schuster, C. F., Bax, D. V., Farndale, R. W., Hamaia, S., Best, S. M., & Cameron, R. E. (2016). Evaluation of cell binding to collagen and gelatin: A study of the effect of 2D and 3D architecture and surface chemistry. *The Journal of Materials Science: Materials, 27*(10), 148.
de Villiers, T. J., & Goldstein, S. R. (2022). Bone health 2022: An update. *Climacteric, 25*(1), 1–3.
Dimitriou, R., Mataliotakis, G. I., Angoules, A. G., Kanakaris, N. K., & Giannoudis, P. V. (2011). Complications following autologous bone graft harvesting from the iliac crest and using the RIA: A systematic review. *Injury, 42*(2), S3–15. Suppl.
Dong, L., Wang, S.-J., Zhao, X.-R., Zhu, Y.-F., & Yu, J.-K. (2017). 3D- printed poly (ε-caprolactone) scaffold integrated with cell-laden chitosan hydrogels for bone tissue engineering. *Scientific Reports, 7*(1), 13412.
Eastell, R., Rosen, C. J., Black, D. M., Cheung, A. M., Murad, M. H., & Shoback, D. (2019). Pharmacological management of osteoporosis in postmenopausal women: An endocrine society* clinical practice guideline. *International Journal of Clinical Endocrinology and Metabolism, 104*(5), 1595–1622.
Ferrari, M., Cirisano, F., & Morán, M. C. (2019). Mammalian cell behavior on hydrophobic substrates: Influence of surface properties. *Colloids Interfaces, 3*.
Fuggle, N. R., Curtis, E. M., Ward, K. A., Harvey, N. C., Dennison, E. M., & Cooper, C. (2019). Fracture prediction, imaging and screening in osteoporosis. *Nature Reviews Endocrinology, 15*(9), 535–547.
Gao, X., Dai, C., Liu, W., Liu, Y., Shen, R., Zheng, X., & Qu, S. (2017). High-scale yield of nano hydroxyapatite through combination of mechanical activation and chemical dispersion. *Journal of Materials Science: Materials in Medicine, 28*(6), 83.
Granfar, R. M., Day, C. J., Kim, M. S., & Morrison, N. A. (2005). Optimised real-time quantitative PCR assays for RANKL regulated genes. *Molecular and Cellular Probes, 19*(2), 119–126.
Halpern, J. M., Urbanski, R., Weinstock, A. K., Iwig, D. F., Mathers, R. T., & von Recum, H. A. (2014). A biodegradable thermoset polymer made by esterification of citric acid and glycerol. *Journal of Biomedical Materials Research Part A, 102*(5), 1467–1477.
Hermanson, G. T. (2013). *Bioconjugate Techniques*. Academic Press.
Hölzl, K., Lin, S., Tytgat, L., Van Vlierberghe, S., Gu, L., & Ovsianikov, A. (2016). Bioink properties before, during and after 3D bioprinting. *Biofabrication, 8*(3), Article 032002.
Islam, M. M., Shahruzzaman, M., Biswas, S., Nurus Sakib, M., & Rashid, T. U. (2020). Chitosan based bioactive materials in tissue engineering applications-A review. *Bioactive Materials, 5*(1), 164–183.
Jing, D., Hao, X., Xu, F., Liu, J., Xu, F., Luo, E., & Meng, G. (2016). Effects of local delivery of BMP2, zoledronate and their combination on bone microarchitecture, biomechanics and bone turnover in osteoporotic rabbits. *Scientific Reports, 6*, 28537.
Kim, J. H., Park, Y. S., Oh, K. J., & Choi, H. S. (2017). Surgical treatment of severe osteoporosis including new concept of advanced severe osteoporosis. *Osteoporos Sarcopenia, 3*(4), 164–169.
Kim, S. E., Suh, D. H., Yun, Y.-P., Lee, J. Y., Park, K., Chung, J.-Y., & Lee, D.-W. (2012). Local delivery of alendronate eluting chitosan scaffold can effectively increase osteoblast functions and inhibit osteoclast differentiation. *Journal of Materials Science: Materials, 23*(11), 2739–2749.
Kimbell, G., & Azad, M. A. (2021). Chapter FIFTEEN - 3D printing: Bioinspired materials for drug delivery. In M. Nurunnabi (Ed.), *Bioinspired, Biomim* (pp. 295–318). Woodhead Publishing.
Ku, J., Seonwoo, H., Park, S., Jang, K.-J., Lee, J., Lee, M., & Chung, J. H. (2020). Cell-laden thermosensitive chitosan hydrogel bioinks for 3D bioprinting applications. *Applied Sciences, 10*(7).
Kylloenen, L., D'Este, M., Alini, M., & Eglin, D. (2015). Local drug delivery for enhancing fracture healing in osteoporotic bone. *Acta Biomaterialia, 11*, 412–434.
Levengood, S. L., & Zhang, M. (2014). Chitosan-based scaffolds for bone tissue engineering. *Journal of Materials Chemistry B, 2*(21), 3161–3184.
Lim, L. Y., Khor, E., & Ling, C. E. (1999). Effects of dry heat and saturated steam on the physical properties of chitosan. *Journal of Biomedical Materials Research, 48*(2), 111–116.
Livak, K. J., & Schmittgen, T. D. (2001). Analysis of relative gene expression data using real-time quantitative PCR and the 2− ΔΔCT method. *Methods, 25*(4), 402–408.
Lusiana, R. A., Siswanta, D., & Mudasir, M. (2016). Preparation of citric acid crosslinked chitosan/poly (vinyl alcohol) blend membranes for creatinine transport. *Indonesian Journal of Chemistry, 16*(2), 144–150.
Ma, R., Yu, Z., Tang, S., Pan, Y., Wei, J., & Tang, T. (2016). Osseointegration of nanohydroxyapatite- or nano-calcium silicate-incorporated polyetheretherketone bioactive composites in vivo. *International Journal of Nanomedicine, 11*, 6023–6033.
Mantha, S., Pillai, S., Khayambashi, P., Upadhyay, A., Zhang, Y., Tao, O., & Tran, S. D (2019). Smart hydrogels in tissue engineering and regenerative medicine. *Materials (Basel, Switzerland), 12*(20).
Marani, P. L., Bloisi, G. D., & Petri, D. F. S. (2015). Hydroxypropylmethyl cellulose films crosslinked with citric acid for control release of nicotine. *Cellulose, 22*(6), 3907–3918.
Martins, C. A., Leyhausen, G., Volk, J., & Geurtsen, W. (2015). Effects of alendronate on osteoclast formation and activity in vitro. *Journal of Endodontics, 41*(1), 45–49.
Maturavongsadit, P., Narayanan, L. K., Chansoria, P., Shirwaiker, R., & Benhabbour, S. R. (2021). Cell-laden nanocellulose/chitosan-based bioinks for 3D bioprinting and enhanced osteogenic cell differentiation. *ACS Applied Bio Materials, 4*(3), 2342–2353.
Maturavongsadit, P., Paravyan, G., Shrivastava, R., & Benhabbour, S. R. (2020). Thermo-/pH-responsive chitosan-cellulose nanocrystals based hydrogel with tunable mechanical properties for tissue regeneration applications. *Materialia, 12*, Article 100681.
McClung, M. (2007). Role of RANKL inhibition in osteoporosis. *Arthritis Research & Therapy, 9*(1), S3. Suppl 1Suppl.
Metwally, S., Ferraris, S., Spriano, S., Krysiak, Z. J., Kaniuk, Ł., Marzec, M. M., & Stachewicz, U. (2020). Surface potential and roughness controlled cell adhesion and collagen formation in electrospun PCL fibers for bone regeneration. *Materials & Design, 194*, Article 108915.
Mizuno, A., Amizuka, N., Irie, K., Murakami, A., Fujise, N., Kanno, T., & Mochizuki, S.-I. (1998). Severe osteoporosis in mice lacking osteoclastogenesis inhibitory factor/osteoprotegerin. *Biochemical and Biophysical Research Communications, 247*(3), 610–615.
Nafee, N., Zewail, M., & Boraie, N. (2018). Alendronate-loaded, biodegradable smart hydrogel: A promising injectable depot formulation for osteoporosis. *Journal of Drug Targeting, 26*(7), 563–575.
Nallusamy, J., & Das, R. K. (2021). Hydrogels and their role in bone tissue engineering: An overview. *Journal of Pharmacy and Bioallied Sciences, 13*(2), S908–s912. Suppl.
Nishio, M., Sugimachi, K., Goto, H., Wang, J., Morikawa, T., Miyachi, Y., & Suzuki, A. (2016). Dysregulated YAP1/TAZ and TGF-β signaling mediate hepatocarcinogenesis in Mob1a/1b-deficient mice. *Proceedings of the National Academy of Sciences of the United States of America, 113*(1), E71–E80.
Owen, R., & Reilly, G. C. (2018). In vitro models of bone remodelling and associated disorders. *Frontiers in Bioengineering and Biotechnology, 6*, 134.
Ozbolat, I. T., Moncal, K. K., & Gudapati, H. (2017). Evaluation of bioprinter technologies. *Additive Manufacturing, 13*, 179–200.
Paspaliaris, V., & Kolios, G. (2019). Stem cells in osteoporosis: From biology to new therapeutic approaches. *Stem Cells International, 2019*.
Pavone, V., Testa, G., Giardina, S. M. C., Vescio, A., Restivo, D. A., & Sessa, G. (2017). Pharmacological therapy of osteoporosis: A systematic current review of literature. *Frontiers in Pharmacology, 8*, 803.
Pedersen, A. B., Heide-Jørgensen, U., Sørensen, H. T., Prieto-Alhambra, D., & Ehrenstein, V. (2019). Comparison of risk of osteoporotic fracture in denosumab vs alendronate treatment within 3 years of initiation. *JAMA Network Open, 2*(4), Article e192416. -e192416.
Petitjean, M., Aussant, F., Vergara, A., & Isasi, J. R. (2020). Solventless Crosslinking of Chitosan, Xanthan, and Locust Bean Gum Networks Functionalized with β-Cyclodextrin. *Gels, 6*(4).
Posadowska, U., Parizek, M., Filova, E., Wlodarczyk-Biegun, M., Kamperman, M., Bacakova, L., & Pamula, E. (2015). Injectable nanoparticle-loaded hydrogel system for local delivery of sodium alendronate. *International Journal of Pharmaceutics, 485*(1–2), 31–40.
Ragetly, G., Griffon, D. J., & Chung, Y. S. (2010). The effect of type II collagen coating of chitosan fibrous scaffolds on mesenchymal stem cell adhesion and chondrogenesis. *Acta Biomaterialia, 6*(10), 3988–3997.
Rahimnejad, M., Adoungotchodo, A., Demarquette, N. R., & Lerouge, S. (2022). FRESH bioprinting of biodegradable chitosan thermosensitive hydrogels. *Bioprinting, 27*, e00209.
Rahimnejad, M., Labonté-Dupuis, T., Demarquette, N. R., & Lerouge, S. (2020). A rheological approach to assess the printability of thermosensitive chitosan-based biomaterial inks. *Biomedical Materials, 16*(1), Article 015003.
Rahmanian-Devin, P., Baradaran Rahimi, V., & Askari, V. R. (2021). Thermosensitive chitosan-β-glycerophosphate hydrogels as targeted drug delivery systems: An overview on preparation and their applications. *Advances in Pharmacological and Pharmaceutical Sciences, 2021*, Article 6640893.
Rajula, M. P. B., Narayanan, V., Venkatasubbu, G. D., Mani, R. C., & Sujana, A. (2021). Nano-hydroxyapatite: A driving force for bone tissue engineering. *Journal of Pharmacy and Bioallied Sciences, 13*(1), S11–s14. Suppl.

Raucci, M. G., Alvarez-Perez, M. A., Demitri, C., Giugliano, D., De Benedictis, V., Sannino, A., & Ambrosio, L. (2015). Effect of citric acid crosslinking cellulose-based hydrogels on osteogenic differentiation. *Journal of Biomedical Materials Research Part A, 103*(6), 2045–2056.

Reid, I. R. (2020). A broader strategy for osteoporosis interventions. *Nature Reviews Endocrinology, 16*(6), 333–339.

Robinson, L. J., Soboloff, J., Tourkova, I. L., Larrouture, Q. C., Witt, M. R., Gross, S., & Blair, H. C. (2021). The function of the calcium channel Orai1 in osteoclast development. *The FASEB Journal, 35*(6), e21653.

Sadeghianmaryan, A., Naghieh, S., Alizadeh Sardroud, H., Yazdanpanah, Z., Afzal Soltani, Y., Sernaglia, J., & Chen, X. (2020). Extrusion-based printing of chitosan scaffolds and their in vitro characterization for cartilage tissue engineering. *International Journal of Biological Macromolecules, 164*, 3179–3192.

Shen, Y., Huang, X., Wu, J., Lin, X., Zhou, X., Zhu, Z., & Shan, P.-F. (2022). The global burden of osteoporosis, low bone mass, and its related fracture in 204 countries and territories, 1990-2019. *Frontiers in Endocrinology, 13*.

Stephens, A. S., Stephens, S. R., & Morrison, N. A. (2011). Internal control genes for quantitative RT-PCR expression analysis in mouse osteoblasts, osteoclasts and macrophages. *BMC Research Notes, 4*, 410.

Takara, E. A., Marchese, J., & Ochoa, N. A. (2015). NaOH treatment of chitosan films: Impact on macromolecular structure and film properties. *Carbohydrate Polymers, 132*, 25–30.

Untergasser, A., Ruijter, J. M., Benes, V., & van den Hoff, M. J. B (2021). Web-based LinRegPCR: Application for the visualization and analysis of (RT)-qPCR amplification and melting data. *BMC Bioinformatics, 22*(1), 398.

Uyanga, K. A., & Daoud, W. A. (2021). Carboxymethyl cellulose-chitosan composite hydrogel: Modelling and experimental study of the effect of composition on microstructure and swelling response. *International Journal of Biological Macromolecules, 181*, 1010–1022.

Wang, W., & Yeung, K. W. K. (2017). Bone grafts and biomaterials substitutes for bone defect repair: A review. *Bioactive Materials, 2*(4), 224–247.

Wilson, S. R., Peters, C., Saftig, P., & Brömme, D. (2009). Cathepsin K activity-dependent regulation of osteoclast actin ring formation and bone resorption. *Journal of Biological Chemistry, 284*(4), 2584–2592.

Włodarczyk-Biegun, M. K., Werten, M. W. T., de Wolf, F. A., van den Beucken, J. J. J. P., Leeuwenburgh, S. C. G., Kamperman, M., & Cohen Stuart, M. A. (2014). Genetically engineered silk–collagen-like copolymer for biomedical applications: Production, characterization and evaluation of cellular response. *Acta Biomaterialia, 10*(8), 3620–3629.

Wu, Q., Therriault, D., & Heuzey, M.-C. (2018). Processing and properties of chitosan inks for 3D printing of hydrogel microstructures. *ACS Biomaterials Science & Engineering, 4*(7), 2643–2652.

Xianmiao, C., Yubao, L., Yi, Z., Li, Z., Jidong, L., & Huanan, W. (2009). Properties and in vitro biological evaluation of nano-hydroxyapatite/chitosan membranes for bone guided regeneration. *Materials Science and Engineering C, 29*(1), 29–35.

Yang, Y., Chen, G., Murray, P., & Zhang, H. (2020). Porous chitosan by crosslinking with tricarboxylic acid and tuneable release. *SN Applied Sciences, 2*(3), 435.

Yang, Y. M., Zhao, Y. H., Liu, X. H., Ding, F., & Gu, X. S. (2007). The effect of different sterilization procedures on chitosan dried powder. *Journal of Applied Polymer Science, 104*(3), 1968–1972.

Zarandona, I., Minh, N. C., Trung, T. S., de la Caba, K., & Guerrero, P. (2021). Evaluation of bioactive release kinetics from crosslinked chitosan films with Aloe vera. *International Journal of Biological Macromolecules, 182*, 1331–1338.

Zhang, Q., Liu, M., Zhou, Y., Liu, W., Shen, J., Shen, Y., & Liu, L. (2013). The effect of alendronate on the expression of important cell factors in osteoclasts. *Molecular Medicine Reports, 8*(4), 1195–1203.

Zhuang, L., Zhi, X., Du, B., & Yuan, S. (2020). Preparation of elastic and antibacterial chitosan–Citric membranes with high oxygen barrier ability by in situ cross-linking. *ACS Omega, 5*(2), 1086–1097.